

Exciton localization in polymers with static disorder

William Barford* and David Trembath

Department of Chemistry, Physical and Theoretical Chemistry Laboratory, University of Oxford, Oxford OX1 3QZ, United Kingdom and Balliol College, University of Oxford, Oxford OX1 3BJ, United Kingdom

(Received 13 July 2009; revised manuscript received 21 August 2009; published 20 October 2009)

Using configuration interaction-singles calculations of realistic models of conjugated polymers and by employing a mapping onto the single-particle Anderson model, we investigate the role of thermally induced static disorder on the properties of excitons in conjugated polymers. We use poly(para-phenylene) as a model system, where the off-diagonal disorder arises from fluctuations in the torsional angles and the diagonal disorder arises from fluctuations in the local relative permittivity. We make the following observations and conclusions: (1) disorder localizes excitons. The exciton localization length defines the exciton conjugation length. (2) Excitons are randomly spatially localized along the chain, with the localization length generally increasing as the excitation energy increases (up to the band center). These define localization or conjugation segments. Generally, the conjugation segments overlap and are not spatially distinct. (3) Triplet excitons are more localized than singlet excitons, because of their smaller band widths. (4) The standard deviation of the Gaussian random disorder, σ , satisfies $\sigma \sim \sqrt{T}$, where T is the temperature. (5) Mapping onto the Anderson model indicates that the conjugation length, $\langle \ell \rangle$, scales as $\langle \ell \rangle \sim \sigma^{-2/3}$ at the edges of the band and $\langle \ell \rangle \sim \sigma^{-3/2}$ at the center of the band. (6) The correlation length of the torsion angles in poly(para-phenylene) scales as σ^{-2} . Thus, there is no direct quantitative correlation between exciton conjugation lengths and conformational disorder. (7) The absorption inhomogeneous line width scales approximately as \sqrt{T} . (8) For realistic values of disorder in poly(para-phenylene) $\langle \ell \rangle \sim 8$ repeat units for the lowest excited singlet and increases to ~ 20 repeat units at the absorption maximum. The absorption line width is ~ 0.5 eV. We use these results to draw further conclusions about electronic processes in conjugated polymers.

DOI: [10.1103/PhysRevB.80.165418](https://doi.org/10.1103/PhysRevB.80.165418)

PACS number(s): 71.20.Rv, 71.35.-y, 71.23.An

I. INTRODUCTION

A conjugated polymer is defined as a chain of molecular repeat units whose π orbitals have nonzero resonance integrals between their nearest neighbors. The nonzero resonance integrals enable the π electrons to delocalize (or conjugate) along the chain. However, at a finite temperature a one-dimensional conjugated polymer is necessarily physically disordered. As to be explained more fully shortly, this disorder disrupts the electronic conjugation.

There are various kinds of physical disorder, including thermally induced large amplitude, low-frequency fluctuations in the torsional (or dihedral) angles between neighboring monomer units and small amplitude, higher frequency intramonomeric vibrations. The former may be regarded as being slow in comparison to electronic time scales, and thus are responsible for static spatial disorder in the electronic couplings. In contrast, the latter are not necessarily slow in comparison to electronic time scales, and thus cause both dynamical and spatial disorder in the electronic couplings.

In addition to physical disorder, as a consequence of the synthesis process, conjugated polymers are also subject to chemical substitution. Also, since a conjugated polymer exists in a liquid or solid-state environment, its electronic properties are determined by the spatial and dynamical fluctuations of the environment. Typically, these will be thermally induced or frozen density fluctuations that change the local relative permittivity (dielectric constant).

Disorder has important implications for the electronic properties of conjugated polymers. As a consequence of a polymer's quasidegeneracy, any quasiparticle is exponentially localized. In a semiconducting polymer a quasiparticle may simply be a doped charge, or, as is the focus of

this paper, it may be an exciton. In this paper we argue that the length scale over which a particle remains phase coherent, namely, the Anderson localization length,¹ defines the electronic conjugation length *for that particle*.

This definition of the conjugation length as a localization length is different from the usual definition found in the literature (see, for example, Ref. 2 and 3). Typically, the conjugation length is defined as the length scale between 'breaks' in the conjugation. The cause of such breaks are often not precisely defined, but it is usually assumed that there is some conformational defect in the polymer that causes the resonance integrals to become smaller than a certain threshold. This picture implies that there is a direct association between the physical conformation of the polymer and its conjugated segments. However, since singlet excitons can delocalize across defects via Coulomb induced resonant exciton transfer, the validity of a threshold in the electronic coupling is questionable.

The conjugation length controls many electronic properties in conjugated polymers. As a number of authors have shown,⁴⁻⁸ the intermolecular exciton transfer integral is a function of the ratio of the conjugation length, ℓ , to the intermolecular separation, D . For conjugation lengths larger than the intermolecular separation, the exciton transfer integral is a decreasing function of the conjugation length. This property has implications for exciton migration. The ground-state London dispersion interaction between polymer chains⁹ is also a function of ℓ/D , scaling as $(\ell/D)^6$ for $\ell \ll D$ and as $(\ell/D)^5$ for $\ell \gg D$.

Disorder also controls the distribution of excited-state energy levels. This, in conjunction with the localization length of the exciton as a function of energy, controls the photo-physical properties of conjugated polymers, for example

causing a temperature dependent inhomogeneous line width.

The observation that the exciton delocalization length is not associated with spatial segmentation in a polymer was made by Beenken and Pullerits¹⁰ via their quantum chemical calculation on disordered polymers. Our definition of the conjugation length as a localization length is consistent with earlier work by Rissler¹¹ and is equivalent to the definition employed by Malyshev and Malyshev¹² in their theoretical investigation of exciton localization in aggregates. Other work on the effects of conformational disorder in conjugated polymers include that by Yaron *et al.*,¹³ who argued that a stiffening of the torsional potential in the excited states accounts for the asymmetry between the absorption and emission spectra of poly(para-phenyleneethylen), and van Averbeke and Beljonne,³ who studied its effects on exciton transport. The role of dynamical dephasing on exciton localization in aggregates has been investigated by Logan and Wolynes.¹⁴

The goal of this paper is to address the effect of static conformational and spatial disorder on the photophysical properties of conjugated polymers. The plan of the paper is as follows. We first study a realistic model of thermally induced disorder in single chains of poly(para-phenylene). We calculate the excited states of the Pariser-Parr-Pople (P-P-P) model for this polymer using the configuration interaction-singles (CI-S) technique.¹⁵ Then using a mapping between the CI-S amplitudes and the exciton two-particle wave function¹⁶ we determine the spread of the center-of-mass wave function. This defines the localization length. We consider two sources of disorder: thermal fluctuations in the torsion angle (i.e., off-diagonal disorder) and thermal fluctuations in the relative permittivity (i.e., diagonal disorder). We find that singlet and triplet excitons have different conjugation lengths: a result that is interpreted via a study of the Anderson model in Sec. III. We also make a preliminary investigation of the effect of disorder on higher-lying excited states.

Next, still using CI-S calculations of the Pariser-Parr-Pople model, we consider model disorder and study the scaling of the conjugation length with disorder. We also investigate the correlation between conformational disorder (in this case determined by the decay of the two-dimensional nematic order parameter) and the localization length.

In Sec. III we map the Pariser-Parr-Pople model onto the single-particle Anderson model. This procedure allows us to study the electronic properties of much larger systems, including the density of excited states and the optical absorption. In addition, it allows us to exploit the large wealth of literature on Anderson localization. We also use this general study to make predictions about the realistic model for poly(para-phenylene) polymers introduced in Sec. II. Finally, we summarize and make concluding remarks in Sec. IV.

II. CI-SINGLES STUDY

In the first part of this section the theoretical models and techniques that are used to characterize exciton localization are introduced. The second part describes the results for exciton localization in poly(para-phenylene) chains.

A. Theoretical background

1. Pariser-Parr-Pople model

The Pariser-Parr-Pople (or extended Hubbard) model is a π -electron model of conjugated polymers, defined by

$$\hat{H} = \sum_i \alpha_i \hat{N}_i - \sum_{\langle ij \rangle \sigma} \beta_{ij} (\hat{c}_{i\sigma}^\dagger \hat{c}_{j\sigma} + \hat{c}_{j\sigma}^\dagger \hat{c}_{i\sigma}), \quad (1)$$

$$+ U \sum_i (\hat{N}_{i\uparrow} - 1/2)(\hat{N}_{i\downarrow} - 1/2) + \frac{1}{2} \sum_{i \neq j} V_{ij} (\hat{N}_i - 1)(\hat{N}_j - 1), \quad (2)$$

where $\langle \rangle$ represents nearest neighbors, $\hat{c}_{i\sigma}^\dagger$ creates a π electron on site i , $\hat{N}_{i\sigma} = \hat{c}_{i\sigma}^\dagger \hat{c}_{i\sigma}$, and $\hat{N}_i = \hat{N}_{i\uparrow} + \hat{N}_{i\downarrow}$.

$\{\alpha_i\}$ and $\{\beta_{ij}\}$ are the Hückel orbital and resonance one-electron integrals, respectively. Conformational and environmental disorder causes spatial and temporal fluctuations in these parameters.

We use the Ohno parameterization for the Coulomb interaction, defined by

$$V_{ij} = U / \sqrt{1 + (U \epsilon_r r_{ij} / 14.397)^2}, \quad (3)$$

where r_{ij} is the interatomic distance (in Å), U is the on-site Coulomb interaction (in eV), and ϵ_r is the relative permittivity. This interaction is an interpolation between an on-site Coulomb repulsion, U , and a Coulomb potential, $e^2 / 4\pi\epsilon_0 r_{ij}$ as $r_{ij} \rightarrow \infty$.

Throughout we use the *screened* parameter set derived by Chandross and Mazumdar¹⁷ to account for solvation effects. These parameters are $U=8$ eV and $\epsilon_r=2$, with $t_p=2.4$ eV and $t_s=2.2$ eV.

2. Definition of exciton conjugation lengths

The simplest description of an exciton in a conjugated polymer is of an electron excited from a set of occupied molecular orbitals (or a valence band) to a set of unoccupied molecular orbitals (or a conduction band) being Coulombically bound to the hole that it leaves behind.^{18–20} This description is also the most relevant for light-emitting polymers. In this picture an exciton is a two-particle object, which (to a good approximation in polymers) is described by two one-particle objects, namely, the center-of-mass particle and the relative particle.

As shown in Ref. 16, there exists a direct mapping from the CI-S amplitudes to the real-space wave function, $\Phi(r, R)$, defined within an appropriately chosen local basis.²¹ Here, R is the center-of-mass coordinate and r is the relative coordinate. $\Phi(r, R)$ can be factorized as,

$$\Phi_{nj}(r, R) = \psi_n(r) \Psi_j(R), \quad (4)$$

where $\psi_n(r)$ is the relative wave function describing the electron-hole pair, and labeled by the principle quantum number n . $\Psi_j(R)$ is the center-of-mass wave function describing the delocalization of the bound pair, and labeled by the pseudomomentum quantum number j .

The exciton wave function serves to define the exciton probability density function,

$$P(r,R) = \frac{\Phi^2(r,R)}{\sum_{r,R} \Phi^2(r,R)}, \quad (5)$$

for the electron-hole separation, r , and position, R .

The size of the electron-hole pair is defined by $2r_{\text{rms}} \equiv 2\sqrt{\langle r^2 \rangle - \langle r \rangle^2}$, where

$$\langle r^n \rangle = \sum_{r,R} P(r,R) r^n. \quad (6)$$

As shown in Fig. 12 of Ref. 16 for poly(para-phenylene), the electron-hole pair is spread over ca. two phenyl repeat units for the $n=1$ family of excitons (the lowest member being the $1B_u$ state). For the $n=2$ family of excitons (the lowest member being the $2A_g$ state) the electron-hole pair is spread over ca. six phenyl repeat units.

Of interest in this paper, however, is the delocalization of the electron-hole pair, i.e., the center-of-mass particle. This is described by the spread of the center-of-mass wave function. Thus, we define the exciton localization length, ℓ , as

$$\ell = 2R_{\text{rms}} \equiv 2\sqrt{\langle R^2 \rangle - \langle R \rangle^2}, \quad (7)$$

where

$$\langle R^n \rangle = \sum_{r,R} P(r,R) R^n. \quad (8)$$

Since the localization length is the length scale over which the exciton retains phase coherence, we argue that the localization length is precisely the exciton conjugation length. With this definition, therefore, the exciton conjugation length is not directly related to the local electronic couplings, unlike the definition used in Ref. 3.

For an ordered polymer ℓ satisfies the particle-in-the-box behavior, defined by

$$\ell = N \sqrt{\frac{\pi^2 j^2 - 6}{3\pi^2 j^2}}, \quad (9)$$

where N is the number of monomers. However, any disorder in one dimension will localize the exciton. The mean center-of-mass coordinate, $\langle R \rangle$, therefore defines the center of the conjugated segment, while ℓ defines its size.

3. Wave-function mapping

The real-space exciton wave function can be obtained directly from a CI-S calculation.^{16,22} The general CI-singles state, $|\frac{1}{3} \psi^{\text{SCI}}\rangle$, is defined as

$$|\frac{1}{3} \psi^{\text{SCI}}\rangle = \sum_{\substack{i \in \text{occupied} \\ j \in \text{unoccupied}}} \psi_i^{\uparrow} \psi_j^{\downarrow}, \quad (10)$$

where the spin-adapted configuration function is

$$|\frac{1}{3} \psi_i^{\uparrow}\rangle = \frac{1}{\sqrt{2}} (\hat{a}_{j\uparrow}^{\dagger} \hat{a}_{i\uparrow} \pm \hat{a}_{j\downarrow}^{\dagger} \hat{a}_{i\downarrow}) |\text{HF}\rangle \quad (11)$$

and ψ_i^{\uparrow} are the configuration function amplitudes. The Hartree-Fock ground state, $|\text{HF}\rangle$, is defined by

$$|\text{HF}\rangle = \prod_{i \in \text{occupied}} \hat{a}_{i\uparrow}^{\dagger} \hat{a}_{i\downarrow}^{\dagger} |0\rangle, \quad (12)$$

where $\hat{a}_{i\sigma}^{\dagger}$ creates an electron in the Hartree-Fock molecular spin orbital, $\chi_{i\sigma}(\mathbf{r})$.

The mapping between the CI-singles amplitudes, ψ_i^{\uparrow} , to the two-dimensional exciton wave function, $\Phi(r,R)$, is described in Ref. 16. To briefly summarize, for a two-band system consisting of occupied orbitals $i \in v$ and unoccupied orbitals $j \in c$,

$$\Phi(r,R) = \sum_{i \in v} \sum_{j \in c} \phi_{R-r/2,i}^v \psi_i^{\uparrow} \phi_{R+r/2,j}^c, \quad (13)$$

where ϕ^v and ϕ^c perform a unitary transformation between the Hartree-Fock delocalized molecular orbitals and localized Wannier functions.

In this paper we are interested in the low-lying ($n=1$) excitons of poly(para-phenylene) (belonging to the A and B_1 irreducible representations for ordered chains). These are predominately caused by particle-hole excitations between the highest band of occupied orbitals of a and b_1 symmetry and the lowest band of unoccupied orbitals, also of a and b_1 symmetry. (These bands are labeled 3 and 4 in Fig. 9 of Ref. 16.) For these bands the transformation functions are

$$\phi_{R,i}^v = \sqrt{\frac{2}{N+1}} \sin\left(\frac{\pi(N-i+1)R}{N+1}\right), \quad (14)$$

and

$$\phi_{R,j}^c = \sqrt{\frac{2}{N+1}} \sin\left(\frac{\pi j R}{N+1}\right), \quad (15)$$

where N is the number of phenyl rings. This transformation means that the exciton is now predominately described as a particle-hole excitation from the highest occupied bonding phenyl-ring molecular orbital to the lowest unoccupied bonding phenyl-ring molecular orbital (labeled 3 and 4 in Fig. 10 of Ref. 16).

4. Origins of off-diagonal disorder

The resonance integral between π -orbitals on neighboring rings i and j is approximately given by

$$\beta_{ij} = \beta_0 \cos \phi_{ij}, \quad (16)$$

where ϕ_{ij} is the torsion angle between the neighboring rings. Thus, for small fluctuations in torsion angle, defined by $\Delta \phi_{ij} = (\phi_j - \phi_i) \ll \phi_0$,

$$\beta_{ij} \approx \beta_0 \cos \phi_0 + \Delta \beta_{ij}, \quad (17)$$

where

$$\Delta \beta_{ij} = -\Delta \phi_{ij} \beta_0 \sin \phi_0. \quad (18)$$

The torsional potential, $V(\phi)$, for a biphenyl molecule is shown in Fig. 1. Close to the global minimum we may expand $V(\phi)$ as

$$V(\phi) = V_0 + \frac{1}{2} K (\phi - \phi_0)^2 + \dots, \quad (19)$$

where

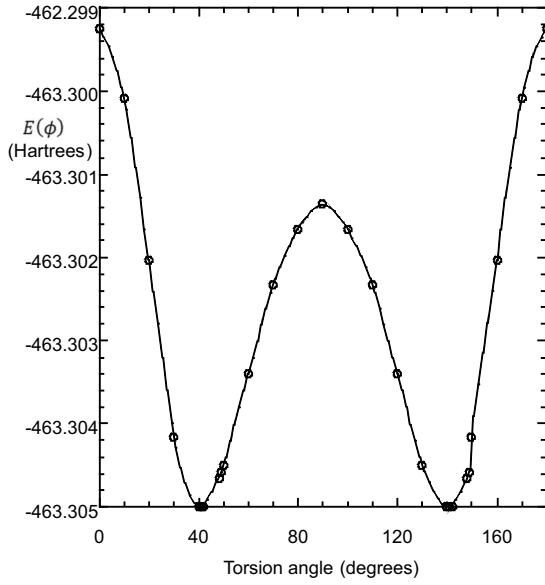


FIG. 1. The torsional potential, $V(\phi)$, for biphenyl determined by the B3LYP DFT functional with the 6-31G(d) basis supplied by GAUSSIAN (Ref. 23).

$$K = \left(\frac{\partial^2 V}{\partial \phi^2} \right)_{\phi=\phi_0}. \quad (20)$$

The probability that the torsion angle lies between ϕ and $\phi+d\phi$ is

$$P(\phi) = \frac{\exp[-V(\phi)/k_B T]}{\int_0^{2\pi} \exp[-V(\phi)/k_B T] d\phi}. \quad (21)$$

The height of the potential barrier shown in Fig. 1 is $\sim 4k_B T$, and therefore it is reasonable to assume that thermal fluctuations only access the harmonic part of the potential close to ϕ_0 . Then, using Eq. (19) in Eq. (21),

$$P(\phi) \approx \left(\frac{K}{2\pi k_B T} \right)^{1/2} \exp(-K(\phi - \phi_0)^2/2k_B T), \quad (22)$$

and thus ϕ is a normally distributed random variable with a standard deviation

$$\sigma_\phi = \left(\frac{k_B T}{K} \right)^{1/2}. \quad (23)$$

According to Eq. (8), therefore, the resonance integral β_{ij} is also a normally distributed random variable whose standard deviation increases as ϕ_0 increases,

$$\sigma_\beta = \beta_0 \sin \phi_0 \left(\frac{k_B T}{K} \right)^{1/2}. \quad (24)$$

Using the computational results shown in Fig. 1, we find that $\phi_0 = 42^\circ$ and $K = 1.13 \text{ eV rad}^{-2}$, implying that $\sigma_\phi = 0.151 \text{ rad}$ at 298 K.

5. Origins of diagonal disorder

Fluctuations in the Hückel Coulomb integral, α , is the origin of diagonal disorder in the Pariser-Parr-Pople model.

To a reasonable approximation we may assume that the valence electrons experience a $1/r$ Coulomb potential with a screened nuclear charge, implying that the Virial theorem is valid. Thus,

$$\alpha \sim -\frac{1}{2} \left(\frac{e^2}{4\pi\epsilon_r\epsilon_0\langle r \rangle} \right), \quad (25)$$

where ϵ_r is the relative permittivity (dielectric constant) of the surrounding medium and $\langle r \rangle$ is the expectation value of the electron radius.

Now, in the continuum limit,²⁴

$$\epsilon_r = \frac{1 + 2\beta'}{1 - \beta'}, \quad (26)$$

where β' is proportional to the mass density, ρ , of the dielectric. Thus, thermal fluctuations in the density of the dielectric cause fluctuations in the relative permittivity. Using Eqs. (25) and (26) and the relation $\rho \sim d^{-3}$, where d is the mean solvent molecular separation, we have

$$\frac{\Delta\alpha}{\alpha} = 2 \frac{(\epsilon_r - 1)(\epsilon_r + 2)}{\epsilon_r} \left(\frac{\Delta d}{d} \right). \quad (27)$$

Assuming a harmonic approximation for the intermolecular interactions, the relative thermal fluctuations in the intermolecular separation are

$$\frac{\Delta d}{d} = \frac{\sqrt{k_B T/C}}{d}, \quad (28)$$

where C is the elastic constant. For a Lennard-Jones potential,

$$V(d) = \frac{A}{d^{12}} - \frac{B}{d^6}, \quad (29)$$

the elastic constant is

$$C = 18 \left(\frac{B^2}{A} \right) \left(\frac{B}{2A} \right)^{1/3}. \quad (30)$$

For benzene at room temperature, $\epsilon_r = 2.27$ and using the tabulated Lennard-Jones parameters²⁵ we find $\Delta d/d \approx 10\%$. Thus, from Eq. (27), $\Delta\alpha/\alpha \approx 25\%$. The ionization potential (i.e., α) of the outer carbon electron is 11.3 eV *in vacuo*. Hence, α for a π electron in a benzene solvent is $\approx 5 \text{ eV}$, and therefore $\Delta\alpha \equiv \sigma_\alpha \approx 1.2 \text{ eV}$. Similarly, for water at room temperature with $\epsilon_r = 78$ and $\Delta d/d \approx 5\%$, we find that $\sigma_\alpha \approx 0.6 \text{ eV}$.

6. Characterizing conformational disorder

One of the goals of this work is to establish whether there exists a direct correlation between the conformational disorder of a polymer and its conjugation lengths. There are various means to describe conformational disorder in a polymer (see, for example, Ref. 26). As fluctuations in the torsional angles of poly(para-phenylene) cause off-diagonal disorder in our model system, we determine the degree of conformational disorder via the correlation of the torsional angles.

Rotations of the phenyl ring by π radians are invariant, so correlations of the phenyl rings separated by j repeat units

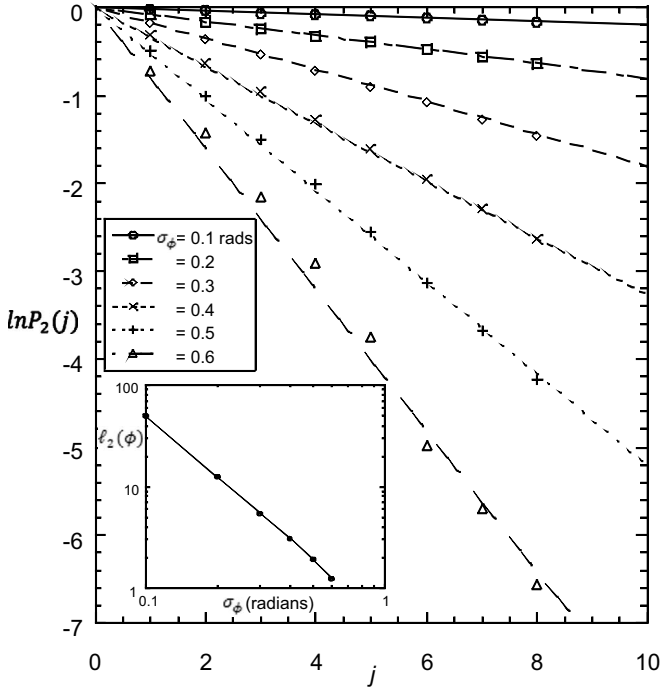


FIG. 2. The statistical correlation of the torsion angles, showing that the two-dimensional nematic order parameter, $P_2(j) \sim \exp[-j/\ell_2(\phi)]$, where j is the separation between rings. The inset shows that $\ell_2(\phi) \sim \sigma_\phi^{-2.0}$.

are characterized by the two-dimensional nematic order parameter, namely,

$$P_2(j) = \frac{1}{N} \sum_i \frac{1}{2} (2 \cos^2 \phi_{i,i+j} - 1). \quad (31)$$

Using our model Gaussian disorder, Fig. 2 shows that the nematic order decays almost exponentially with the separation between phenyl rings. Using the nematic correlation length, $\ell_2(\phi)$, extracted from Fig. 2, the inset of Fig. 2 shows that $\ell_2(\phi)$ scales with disorder as $\ell_2(\phi) \sim \sigma_\phi^{-2.0}$. As shown in Sec. III, this scaling behavior is different from that of the localization lengths.

B. Results

1. Realistic disorder

We now turn to discuss the exciton conjugation lengths in poly(para-phenylene) for realistic estimates of disorder for polymers in a hydrocarbon solvent. CI-S calculations of the Pariser-Parr-Pople model are performed using an efficient Direct-CI method.^{16,27} We use the parameters derived in Secs. II A 4 and II A 5, namely, $\phi_0=42^\circ$, $K=1.13$ eV rad⁻², $\sigma_\phi=0.151$ rad., and $\sigma_\alpha=0.5-1.0$ eV. We consider the $n=1$ family of excitons.

Figure 3 shows the localization length, $\langle \ell \rangle$, averaged over 40 realizations of the disorder versus the inverse chain length (where the angular brackets mean an average over disorder and N is the number of phenyl rings). These results are for the lowest excited singlet and triplet excitons. For fixed off-diagonal disorder, the localization length decreases as the

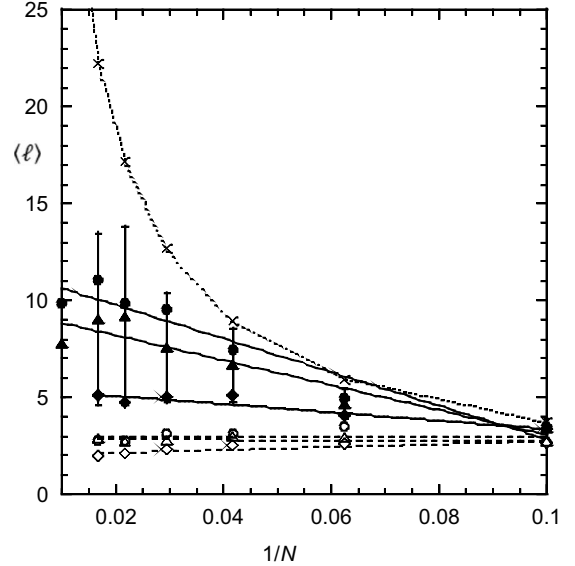


FIG. 3. The exciton localization length, $\langle \ell \rangle$, in units of the repeat distance versus the inverse chain length (where N is the number of phenyl rings) averaged over 40 realizations of the disorder. Singlets (filled symbols and solid curves) and triplets (empty symbols and dashed curves). $\phi_0=42^\circ$ and $\sigma_\phi=0.151$ rad; $\sigma_\alpha=0$ (circles), $\sigma_\alpha=0.5$ eV (triangles), and $\sigma_\alpha=1.0$ eV (diamonds). The standard deviation of $\langle \ell \rangle$ at $N=60$ when $\sigma_\alpha=0.5$ eV is 4.5 repeat units, while the standard error of the mean is 0.7 repeat units. For the ordered chain (crosses and dashed curve) ℓ satisfies the particle-in-the-box expression, $\ell = N\sqrt{(\pi^2-6)}/3\pi^2$.

diagonal disorder increases. The error bars on the $\sigma_\alpha=0.5$ eV singlet exciton result indicate the large fluctuations in the localization length for a particular realization of the disorder. In general, $\Delta\langle \ell \rangle \sim O(\langle \ell \rangle)$.

For a realistic value of $\sigma_\alpha \sim 0.5$ eV the converged singlet localization length is ~ 10 repeat units. The triplet localization length is considerably smaller, being $\sim 2-3$ repeat units. As explained in Sec. III, this difference can be understood via the single parameter scaling theory derived from an analysis of the Anderson model. Generally, the localization length satisfies $\langle \ell \rangle \sim (D/W)^{-\nu}$, where D and W are the energy scales for the disorder and the exciton band width, respectively, and ν is an energy-dependent exponent. When $\sigma_\alpha=0$ the disorder energy scale is the same for both singlet and triplet excitons. However, the singlet exciton band width is larger, as singlets delocalize by both charge-transfer mechanisms and Coulomb induced resonant exciton transfer, while triplets only delocalize via charge-transfer mechanisms. A theoretical analysis of these mechanisms will be given in Sec. III. For now, we make a computational estimate of the exciton band width by assuming that the excitation energy satisfies the particle-in-the-box expression,

$$\Delta E_j = E_\infty - 2\beta_{\text{exciton}} \cos\left(\frac{\pi j}{(N+1)}\right), \quad (32)$$

where $W_{\text{exciton}}=4\beta_{\text{exciton}}$. Equating $(\Delta E_2 - \Delta E_1)$ with the difference in excitation energies between the two lowest excitations as a function of N and extrapolating to $N \rightarrow \infty$ implies

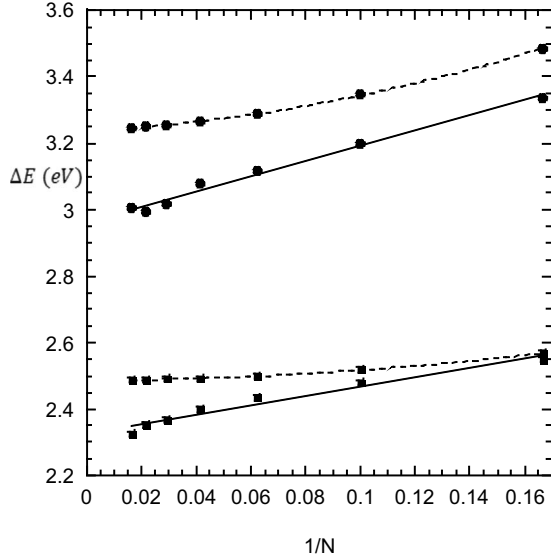


FIG. 4. Lowest-lying singlet (circles) and triplet (squares) excitation energies for poly(para-phenylene) versus inverse chain length (where N is the number of phenyl rings). $\sigma_\phi=0.151$ rad and $\sigma_\alpha=1.0$ eV (solid curves), ordered chain (dashed curves).

that $\beta_{\text{exciton}}=3.72$ eV for singlets, while $\beta_{\text{exciton}}=0.86$ eV for triplets. These results will be used in Sec. III to map the Pariser-Parr-Pople model onto the Anderson model.

Figure 4 shows the disorder averaged excitation energy of the lowest singlet and triplet excitons versus inverse chain length for $\sigma_\alpha=1$ eV. In comparison to the excitation energies in an ordered chain, which exhibits $1/N^2$ scaling as $N \rightarrow \infty$, the disordered chains appear to exhibit $1/N$ scaling. This result, however, is an artifact of the particular parameters used and the small range of length scales. The correct scaling behavior is discussed in Sec. III.

We now turn to a preliminary discussion of the effect of disorder on the higher-lying excited states. Figure 5 shows the energy spectrum and localization lengths of singlet excited states for two particular realizations of the disorder for a 50-ring chain. Figure 5(b) in particular shows a number of interesting features. First, the localization length generally increases as the excitation energy increases. Second, although the mean position of the excitons is on different parts of the chain, the localization lengths generally overlap. We interpret these regions as localization or conjugation segments. We therefore see that it is not reasonable to assume spatially *separate* conjugated segments (as is the usual assumption).

Finally, Fig. 5(b) shows the oscillator strengths (normalized relative to the lowest-lying singlet). The behavior is quite different to that of an ordered chain, where the oscillator strength is predominately carried by the lowest-lying exciton. For a disordered chain, in contrast, a number of states have significant oscillator strength. The center-of-mass wave functions, $\Psi_j(R) \equiv \Phi_{n=1,j}(r=0, R)$, of a number of excitations are shown in Fig. 6. The four lowest states are spatially quite separate, with small probability amplitudes in the vicinity of the nodes of their wave functions. This picture conforms to the concept of “local ground states” proposed by Malyshev and Malyshev.¹² However, the 9th. excitation violates this

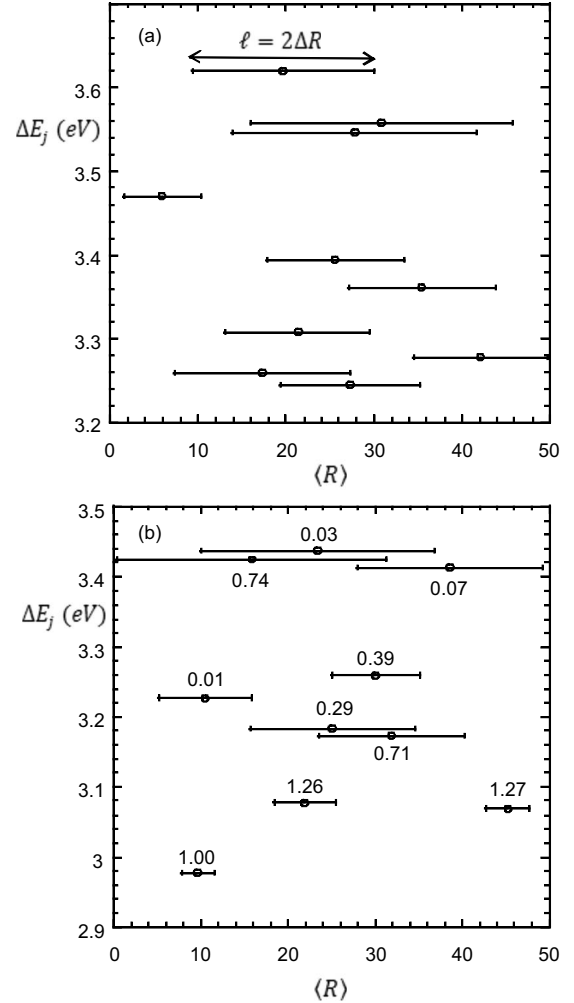


FIG. 5. Singlet excitation energies, localization lengths and oscillator strengths normalized to the $j=1$ value for a 50-ring poly(para-phenylene) chain. (a) $\sigma_\phi=0.151$ rad and $\sigma_\alpha=0$; (b) $\sigma_\phi=0.151$ rad and $\sigma_\alpha=1.0$ eV. Lengths are in units of the repeat distance. The horizontal bars may be interpreted as energy-dependent conjugated segments.

concept, as it also has a large oscillator strength, but its wave function overlaps those of the lowest four excitations. The role of disorder on the inhomogeneous line width is described in Sec. III.

2. Model disorder

In this section we treat the disorder in the torsion angle as a model parameter. To represent the average torsion angle in the solid state, we set $\phi_0=27.4^\circ$. Diagonal disorder is neglected.

Figures 7 and 8 show the average localization length, $\langle \ell \rangle$, for the lowest-lying singlet and triplet exciton, respectively. These results are obtained by averaging over 40 realizations of the disorder. As found before, increased disorder increases the localization and the triplet excitons are more localized than the singlet excitons.

For $\sigma_\phi \geq 0.3$ rad $\langle \ell \rangle$ has converged at 60 rings for the singlet excitons. These converged results are plotted against

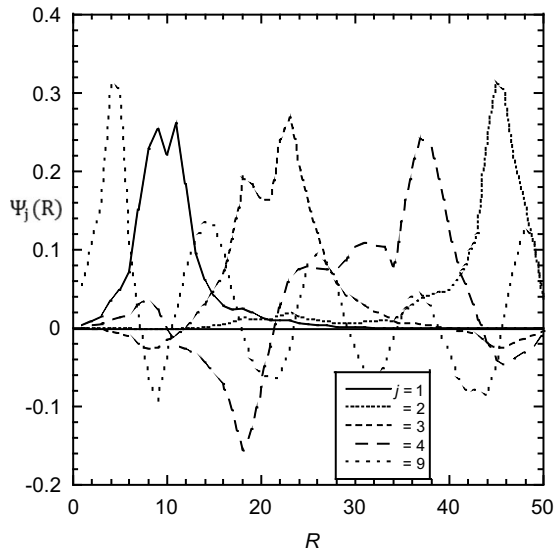


FIG. 6. The exciton center-of-mass wave function, $\Psi_j(R)$, for some of the excitons shown in Fig. 5(b).

$\ell_2(\phi)$ in Fig. 9, showing a qualitative correlation between conformational disorder and the conjugation length. The range of length scales is too small in these calculations to obtain a scaling relation. However, as discussed in Sec. III, $\langle \ell \rangle$ is expected to scale as $\sigma_\phi^{-2/3}$ for the lowest-lying exciton, whereas $\ell_2(\phi)$ scales as σ_ϕ^{-2} . Thus, any correlation between conformational disorder and conjugation lengths is only qualitative.

We conclude this section by noting that excited states planarize the molecule and change the stiffness of the torsional potential, which in turn alters the off-diagonal disorder.

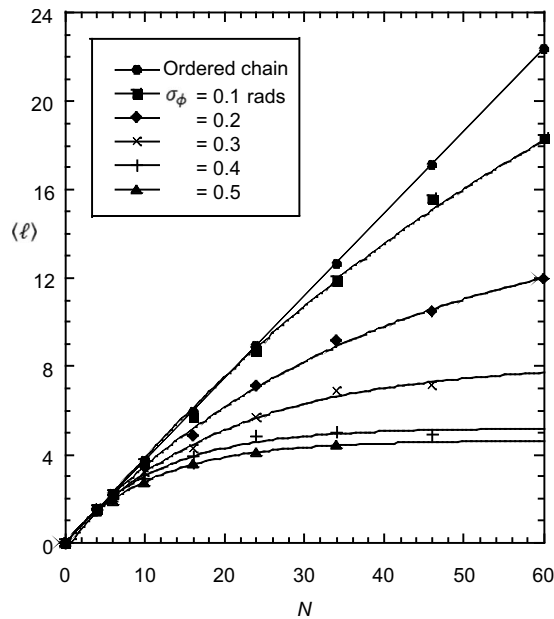


FIG. 7. The singlet exciton localization length, $\langle \ell \rangle$, in units of the repeat distance versus inverse chain length (where N is the number of phenyl rings) averaged over 40 realizations of the disorder. $\phi_0=27.4^\circ$ and $\sigma_\alpha=0$. For the ordered chain ℓ satisfies the particle-in-the-box expression, $\ell=N\sqrt{(\pi^2-6)}/3\pi^2$.

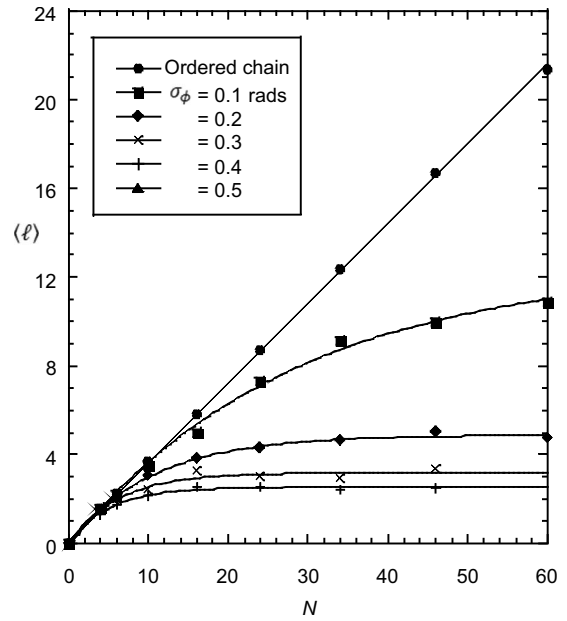


FIG. 8. As for Fig. 7 for the triplet exciton localization length.

Competing with that effect is the intrinsic self-trapping of the exciton. Thus, the affect on exciton localization of electron-lattice coupling is a subtle one, and under current investigation.

III. ANDERSON MODEL STUDY

The computational expense of the CI-S method means that it is only possible to study the effects of disorder in poly(para-phenylene) chains of up to 100 repeat units. Although this is long enough to make reasonable predictions of realistic conjugations lengths, it is too short to make any

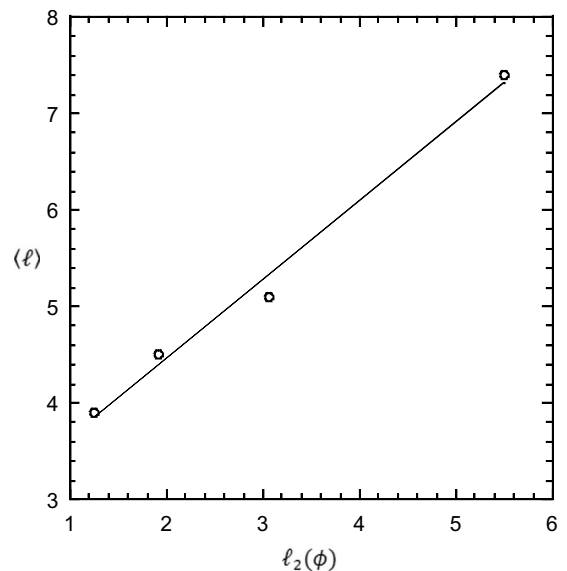


FIG. 9. Correlation between the singlet localization length, $\langle \ell \rangle$, versus the correlation length of the torsion angle, $\ell_2(\phi)$. Lengths are in units of the repeat distance.

scaling predictions. Furthermore, it is not possible to perform many ensemble averages over excited states to determine the photophysical properties. However, since we are largely concerned with the electronic properties arising from the delocalization of the center-of-mass particle, further insight can be achieved by mapping the Pariser-Parr-Pople model onto an effective one-particle Hamiltonian. In the context of disorder, this model is generally known as the Anderson model.¹

A. Effective exciton Hamiltonian

The goal of this section is to derive an effective low-energy exciton Hamiltonian starting from the Pariser-Parr-Pople Hamiltonian. To achieve this goal it is convenient to partition the Pariser-Parr-Pople Hamiltonian into an intraphenyl-ring component, H^{intra} , and an interphenyl-ring component, H^{inter} ,

$$H = H^{\text{intra}} + H^{\text{inter}}. \quad (33)$$

The Hilbert space of particle-hole excitations is spanned by the basis functions¹⁶ $\{|m, \Delta m\rangle\}$, which represent a particle excited from a localized occupied basis state on the phenyl ring at $(m - \Delta m/2)$ to a localized vacant basis state on the phenyl ring at $(m + \Delta m/2)$. As shown in Fig. 12 of Ref. 16, the lowest family of excitons (i.e., $n=1$) consist of particle-hole excitations whose average particle-hole separation is approximately one to two phenyl rings. For these family of excitons, therefore, we may assume to zeroth order that the Hilbert space is spanned by the basis functions $\{|m, 0\rangle\}$. We will describe this family of excitons as intraring excitations (or Frenkel excitons). The basis functions $\{|m, \Delta m\rangle\}$ describe charge-transfer excitons separated by Δm repeat units.

The intraring excitations are described by H^{intra} , while H^{inter} describes interring excitations, as well as the delocalization of excitations along the polymer chain. There are two components of H^{inter} that result in different mechanisms for delocalization of the intraring excitations.

First, the kinetic-energy term of H^{inter} leads to nearest-neighbor hopping via a virtual excited state corresponding to charge transfer between neighboring rings (i.e., to the basis functions $\{|m, 1\rangle\}$). The energy scale for this is

$$\beta_{\text{exciton}}^{\text{KE}} = \frac{\tilde{\beta}^2}{\tilde{U} \pm \tilde{J} - \tilde{V}}, \quad (34)$$

where the tilde refers to molecular-orbital parameters derived from the Pariser-Parr-Pople model parameters. \tilde{U} and \tilde{V} are the Coulomb repulsion between a pair of electrons on the same ring and neighboring ring, respectively, while $\tilde{\beta}$ is the highest occupied molecular orbital–lowest unoccupied molecular orbital phenyl-ring hybridization integral. $2\tilde{J}$ is the spin-exchange interaction, where the positive sign refers to triplets and the negative sign refers to singlets. Thus, as a consequence of their stronger electron-hole binding, the effective delocalization energy, $\beta_{\text{exciton}}^{\text{KE}}$, is smaller for triplets.

The second component of H^{inter} , namely, the Coulomb potential, causes long-range exciton delocalization via reso-

nant exciton transfer. For the lowest family of excitons the transition dipole moments are oriented along the molecular axis. Thus, within the point-dipole moment approximation,

$$\beta_{\text{exciton}}^{\text{PE}} = \frac{2\mu_1}{R_{ij}^3}, \quad (35)$$

where μ_1 is the transition dipole moment for the intramolecular excitation and R_{ij} is the distance between rings i and j . Since μ_1 vanishes for triplet excitations, this is a second reason why the overall exciton delocalization integral,

$$\beta_{\text{exciton}} = \beta_{\text{exciton}}^{\text{KE}} + \beta_{\text{exciton}}^{\text{PE}}, \quad (36)$$

is smaller for triplet excitons than for singlet excitons, as confirmed by the computational result given in Sect. II B 1. The exciton bandwidth is $4\beta_{\text{exciton}}$.

B. Localization in the effective exciton Hamiltonian

The delocalization of the exciton center-of-mass particle is described by the single-particle Anderson model (or disordered Hückel model), defined for open systems by

$$H = \sum_{n=1}^N \alpha_n |n\rangle\langle n| - \sum_{n=1}^{N-1} \{\beta_n (|n\rangle\langle n+1| + |n+1\rangle\langle n|)\}, \quad (37)$$

with β_n defined by Eq. (36). Here, the site index n is equivalent to the repeat unit index m of the Pariser-Parr-Pople model.²⁸ The properties of Eq. (37) have been extensively studied in one and higher dimensions. It is well established that in one dimension disorder causes exponential localization of the particle wave function (see Ref. 29 for a review).

In the present work $\{\beta_n\}$ and $\{\alpha_n\}$ are taken to be Gaussian random variables, with mean values of $\beta=1$ and $\alpha=4$, and standard deviations of σ_β and σ_α . The groundstate of Eq. (37) corresponds to the lowest-lying exciton, while its excitations correspond to higher-lying excitons.

Since for triplet excitons the bandwidth is determined by the value of β_{ij} in the P-P-P model, we can make a direct connection between this model and the realistic parameters used in Sec. II B 1. There, we took $\phi_0=42^\circ$ and $\sigma_\phi=0.151$ rad. Now, according to Eqs. (17) and (8),

$$\left(\frac{D}{W}\right)_{\text{P-P-P model}} \equiv \left|\frac{\Delta\beta_{ij}}{\beta_0}\right| = \Delta\phi_{ij} \tan \phi_0 \equiv \sigma_\phi \tan \phi_0. \quad (38)$$

However, from the discussion above on effective triplet exciton band widths [see Eq. (34)], we see that

$$\left(\frac{\Delta\beta}{\beta}\right)_{\text{exciton model}} = 2 \left(\frac{\Delta\beta}{\beta}\right)_{\text{P-P-P model}}, \quad (39)$$

and thus,

$$\left(\frac{\sigma_{\beta_{\text{exciton}}^{\text{triplet}}}}{\beta_{\text{exciton}}^{\text{triplet}}}\right) = 2\sigma_\phi \tan \phi_0 = 0.272. \quad (40)$$

For the singlet excitons, however,

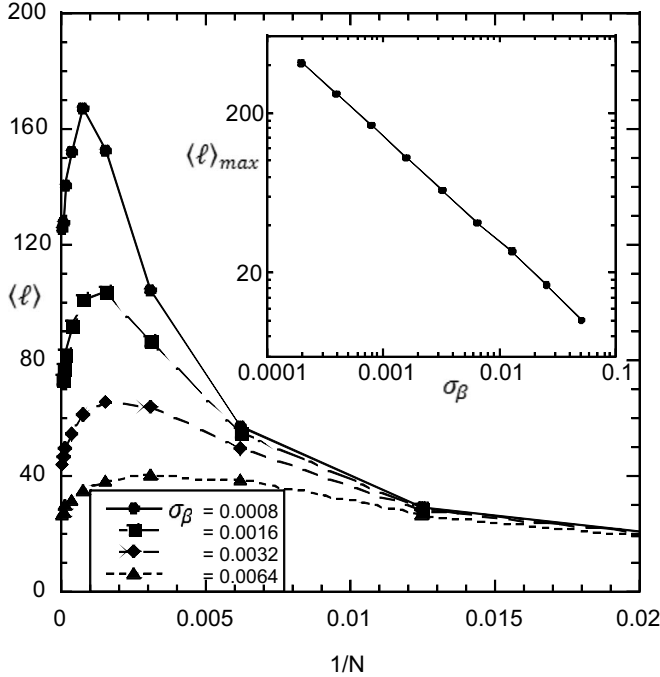


FIG. 10. The ground-state localization length, $\langle \ell \rangle$, in units of the repeat distance for the Anderson model with N sites averaged over 1000 realizations of the disorder (with $\sigma_\alpha=0$). The inset shows that $\langle \ell \rangle \sim \sigma_\beta^{-2/3}$.

$$\left(\frac{\sigma_\beta^{\text{singlet}}}{\beta_{\text{exciton}}^{\text{singlet}}} \right) = \left(\frac{\beta_{\text{exciton}}^{\text{triplet}}}{\beta_{\text{exciton}}^{\text{singlet}}} \right) \left(\frac{\sigma_\beta^{\text{triplet}}}{\beta_{\text{exciton}}^{\text{triplet}}} \right) = 0.065, \quad (41)$$

using the values of $\beta_{\text{exciton}}^{\text{singlet}}$ and $\beta_{\text{exciton}}^{\text{triplet}}$ from Sec. II B 1. Thus, defining all energy scales in the Anderson model by either $\beta_{\text{exciton}}^{\text{singlet}}$ or $\beta_{\text{exciton}}^{\text{triplet}}$ (i.e., setting $\beta_{\text{exciton}}^{\text{singlet}} = \beta_{\text{exciton}}^{\text{triplet}} = \beta = 1$), the dimensionless realistic values of the off-diagonal disorder are $\sigma_\beta^{\text{triplet}} = 0.272$ and $\sigma_\beta^{\text{singlet}} = 0.065$.

1. Lowest excited-state exciton properties

The lowest excited-state exciton corresponds to the ground state of Eq. (37). This is computed via sparse-matrix diagonalization (e.g., the conjugate gradient method³⁰). As before, the size of the single-particle wave function, $\ell = 2\Delta R$, is taken as a measure of the delocalization length. Taking $\sigma_\beta = 0.272$ on a 60-site chain (to model the triplet excitons on a 60-ring poly(para-phenylene) chain) gives $\langle \ell \rangle = 3.4$, while taking $\sigma_\beta = 0.065$ (to model the singlet excitons) gives $\langle \ell \rangle = 8.9$. These results are remarkably consistent with the CI-S analysis shown in Fig. 3, confirming the validity of the mapping onto the Anderson model.

Figure 10 shows $\langle \ell \rangle$ versus the inverse number of sites, N , for various values of the disorder in β averaged over 1000 realizations of the disorder. Evidently, $\langle \ell \rangle$ shows a maximum value as a function of $1/N$. Defining this maximum value as $\langle \ell \rangle_{max}$, the inset of Fig. 10 shows that $\langle \ell \rangle_{max} = 1.14\sigma_\beta^{-2/3}$, in agreement with Ref. 12. (The same scaling is also obtained if the value of $\langle \ell \rangle$ obtained by extrapolating to $N \rightarrow \infty$ is used.) A calculation for various values of the disorder in α shows that $\langle \ell \rangle_{max} = 2.28\sigma_\alpha^{-2/3}$

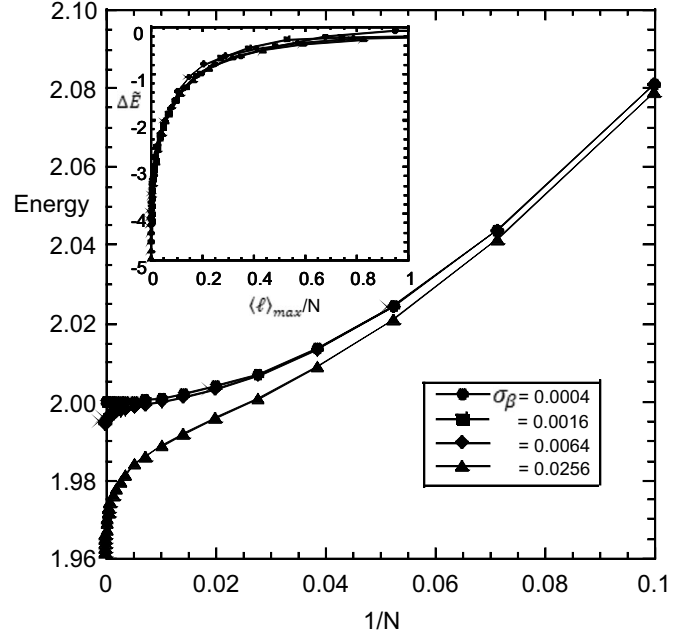


FIG. 11. The ground-state energy in units of β for the Anderson model with N sites averaged over 10 000 realizations of the disorder (with $\sigma_\alpha=0$). The inset shows $\Delta \tilde{E} = (E_{\sigma_\beta}^{GS}(N) - E_{\sigma_\beta=0}^{GS}(N)) / \langle \Delta E_{rms}(\langle \ell \rangle_{max}) \rangle$ versus $\langle \ell \rangle_{max}/N$.

Figure 11 shows the groundstate energy as a function of $1/N$ averaged over 10 000 realizations of the disorder. For the weakest disorder $E(N)$ appears to show $1/N^2$ scaling. For the strongest disorder, however, there is a clear change in curvature for large N , while there is $\sim 1/N$ scaling for intermediate chain lengths. This downward curvature in energy is because in the asymptotic limit particles can explore regions of the chain of the size of the localization length where locally the values of $\{\beta_n\}$ are all increased from the average, thus decreasing their kinetic energy. A single parameter scaling is still relevant, as by an appropriate scaling the data collapses onto a universal curve. We define a scaled deviation in energy from the ordered chain as,

$$\Delta \tilde{E} = \frac{(E_{\sigma_\beta}^{GS}(N) - E_{\sigma_\beta=0}^{GS}(N))}{\langle \Delta E_{rms}(\langle \ell \rangle_{max}) \rangle}, \quad (42)$$

where $\langle \Delta E_{rms}(\langle \ell \rangle_{max}) \rangle$ is the disorder averaged root-mean-square deviation in the ground-state energy at $N = \langle \ell \rangle_{max}$. Then, as the inset to Fig. 11 shows, $\Delta \tilde{E}$ is a universal function of the scaled inverse length, namely, $\langle \ell \rangle_{max}/N$. We note that exciton emission energies will not necessarily show this behavior, as the radiative lifetime of the exciton is too short for it to explore all the energetically favorable conjugation segments. A full study of the emission spectrum requires a detailed kinetic simulation that lies outside the scope of this paper.

2. Excited state exciton properties

Equation (37) is a useful model for investigating the photophysical properties of conjugated polymers. Excited states are easily calculated in this one-particle Hamiltonian,³¹ lead-

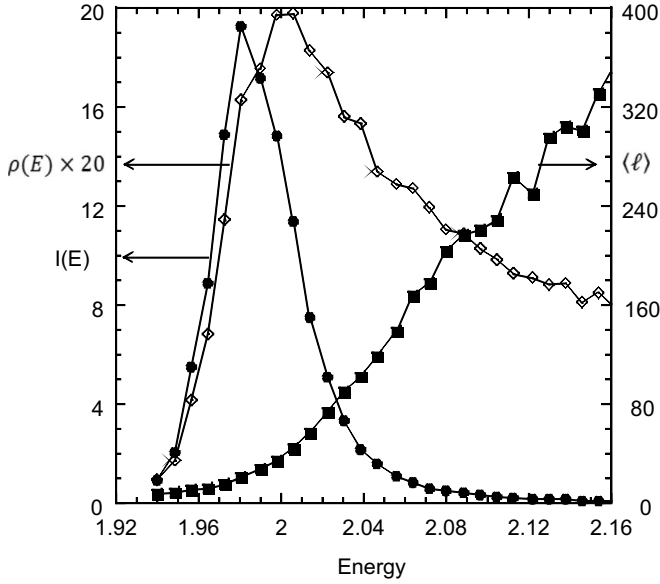


FIG. 12. Results for excited states of the Anderson model with 10 000 sites, $\sigma_\beta=0.04$ and $\sigma_\alpha=0$, averaged ten realizations of the disorder. The energy is in units of β . Optical absorption, $I(E)$, normalized such that $\int I(E)dE=1$ (filled circles); density of states, $\rho(E)$, normalized such that $\int \rho(E)dE=1$ (empty diamonds); localization length, $\langle \ell \rangle$, in units of the repeat distance (filled squares).

ing to a calculation of $\langle R_j \rangle$ and ℓ_j for the excited state j . Oscillator strengths are also easily evaluated, as the transition dipole moment of the j th state for N sites is^{8,10}

$$\mu_j = \mu_1 \sum_{n=1}^N \Psi_j(n), \quad (43)$$

where μ_1 is the transition dipole moment for the intramolecular excitation and $\Psi_j(n)$ is the single-particle wave function.

The optical absorption, $I(E)$, is defined by

$$I(E) = \sum_j f_j \delta(E - E_j) \quad (44)$$

where the oscillator strength is

$$f_j \sim E_j \mu_j^2 \quad (45)$$

and normalized such that

$$\sum_{j=1}^N f_j = N. \quad (46)$$

Figure 12 shows the normalized optical absorption, $I(E)$, for $N=10\,000$ averaged over 10 realizations of the disorder. Here, $\sigma_\beta=0.04$ and $\sigma_\alpha=0$. This value of σ_β is chosen because for long chains it predicts a localization length for the lowest exciton of eight repeat units, in good qualitative agreement with Sec. II B 1.

The figure shows that the initial increase in $I(E)$ is associated with the increase in the density of states, $\rho(E)$. Indeed, the density of states shows a distribution that qualitatively

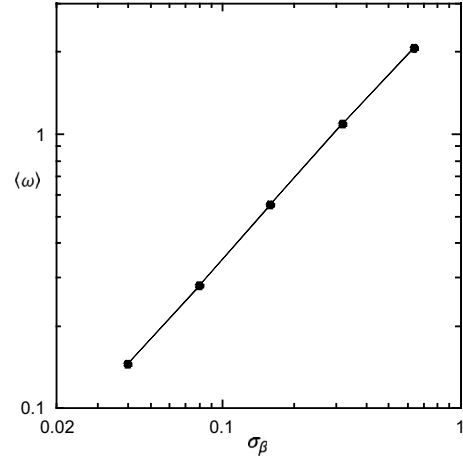


FIG. 13. The absorption line width in units of β versus σ_β , showing that $\langle \omega \rangle \sim \sigma_\beta^{0.96}$.

justifies the Gaussian random disorder model,³² and is quite different from that of an ordered chain in which

$$\rho(E) = \frac{1}{\pi(4\beta^2 - E_j^2)^{1/2}}, \quad (47)$$

where

$$E_j = \alpha - 2\beta \cos\left(\frac{\pi j}{N+1}\right) \quad (48)$$

and $\rho(E)$ is normalized such that

$$\int \rho(E)dE = 1. \quad (49)$$

As shown in Fig. 13, the inhomogeneous line width (defined as twice the standard deviation of the optical absorption) scales as $\langle \omega \rangle \approx 3.2\sigma_\beta^{0.96}$ (in units of β). Since for thermally induced disorder, $\sigma \sim \sqrt{T}$, we therefore predict that the inhomogeneous line width should approximately scale as \sqrt{T} . It is also instructive to use this model to predict the line width in poly(para-phenylene). Using $\sigma_\beta=0.04$ gives $\langle \omega \rangle = 0.14\beta$, and setting $\beta = \beta_{\text{exciton}}^{\text{singlet}} = 3.72$ eV (as derived in Sec. II B 1) gives $\langle \omega \rangle \sim 0.5$ eV at 298 K.

Figure 12 also shows the energy-dependent localization lengths. At the onset of the absorption $\langle \ell \rangle \sim 8$, while at the absorption peak $\langle \ell \rangle \sim 20$. This increase of localization length with energy is consistent with the CI-S study shown in Fig. 5(b). It also suggests that a high-lying exciton (whether photoexcited or formed via electron-hole recombination) relaxes energetically by migrating to conjugated segments of progressively shorter lengths. This is in contrast to the received wisdom that excitons relax by migrating to longer conjugated segments.

The full energy dependence of the localization length is shown in Fig. 14. At the band edges this calculation confirms our earlier prediction that $\langle \ell \rangle \sim \sigma_\beta^{-2/3}$, while near the band center $\langle \ell \rangle \sim \sigma_\beta^{-3/2}$, in agreement with localization lengths derived from the Lyapunov exponent.²⁹

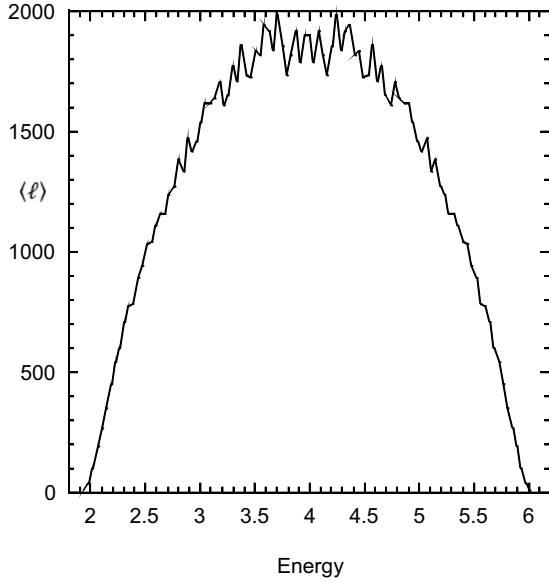


FIG. 14. The localization length, $\langle \ell \rangle$ (in units of the repeat distance) of the Anderson model as a function of energy (in units of β) with 10 000 sites, $\sigma_\beta=0.04$, averaged over ten realizations of the disorder. At the band edges, $\langle \ell \rangle \sim \sigma_\beta^{-2/3}$, while near the band center $\langle \ell \rangle \sim \sigma_\beta^{-3/2}$.

IV. CONCLUSIONS

Using CI-S calculations of realistic models of conjugated polymers and by employing a mapping onto the single-particle Anderson model, this paper has described the role of thermally induced static disorder on excitons in conjugated polymers. We make the following observations:

(1) disorder localizes excitons. The exciton localization length *defines* the exciton conjugation length;

(2) excitons are randomly spatially localized along the chain, with the localization length generally increasing as the excitation energy increases (up to the band center). These regions define localization or *conjugation segments*. Generally, the conjugation segments overlap and are not spatially distinct. (This trivially explains why intrachain exciton migration is more efficient in more ordered chains.)

(3) Triplet excitons are more localized than singlet excitons because of their smaller band widths;

(4) within the harmonic approximation, the standard deviation of the Gaussian random disorder satisfies $\sigma \sim \sqrt{T}$, where T is the temperature;

(5) mapping the Pariser-Parr-Pople model onto the Anderson model indicates that the conjugation length, $\langle \ell \rangle$, scales as $\langle \ell \rangle \sim \sigma^{-2/3}$ at the edges of the band and $\langle \ell \rangle \sim \sigma^{-3/2}$ at the center of the band.

(6) the correlation length of the torsion angles in poly(para-phenylene) scales as σ^{-2} . Thus, there is no *direct* quantitative correlation between localization lengths and conformational disorder;

(7) the absorption inhomogeneous line width scales approximately as \sqrt{T} ; and

(8) for realistic values of disorder in poly(para-phenylene) $\langle \ell \rangle \sim 8$ repeat units for the lowest excited singlet and increases to ~ 20 repeat units at the absorption maximum. The absorption line width is ~ 0.5 eV.

An important conclusion that can be drawn from this work is that our assumption that the exciton localization length defines its conjugation length leads to a quite different description of exciton dynamics in conjugated polymers. According to the usual assumption that conjugated segments are spatially distinct, each supporting a local energetic spectrum of excited states, a high-lying exciton will typically migrate through the polymer by hopping to different spatial regions with increasing conjugation lengths. In our picture, on the other hand, conjugated segments are energetically distinct, but in general spatially overlapping. In this case a high-lying exciton will migrate through the polymer by energetically relaxing to conjugated segments that may spatially overlap its initial segment. Furthermore, as it relaxes it will get more, not less localized. These different scenarios can in principle be distinguished by experimental studies of exciton dynamics or by the temperature dependency of the inhomogeneous line widths. For example, if we assume that the exciton conjugation length, ℓ , is a conformational persistence length, then it is easy to show that

$$\frac{\Delta E}{E} \sim \left(\frac{\Delta \ell}{\ell} \right) \frac{1}{\ell}, \quad (50)$$

for $1 \ll \ell \ll \infty$, and

$$\frac{\Delta E}{E} \sim \left(\frac{\Delta \ell}{\ell} \right) \frac{1}{\ell^2}, \quad (51)$$

as $\ell \rightarrow \infty$. Thus, in the case of two-dimensional nematic order, where $\Delta \ell = \sqrt{2} \ell$ and $\ell \sim \sigma^{-2} \sim T$, $\Delta E/E \sim T^2$ as $T \rightarrow 0$, while $\Delta E/E \sim T$ as $T \rightarrow \infty$.

Finally, we note that this study has only considered static disorder. Temporal disorder, as well as exciton self-trapping, is also responsible for exciton localization, and these are under current investigation.

ACKNOWLEDGMENTS

W.B. acknowledges the financial support of the EPSRC (UK) (Grant No. EP/D038553/1) and the John Fell Fund of the University of Oxford. We also thank Nattapong Paiboonvorachat for supplying us with his CI-S code.

*william.barford@chem.ox.ac.uk

- ¹P. W. Anderson, Phys. Rev. **109**, 1492 (1958).
- ²G. D. Scholes and G. Rumbles, Nature Mater. **5**, 683 (2006).
- ³R. van Aaverbeke and D. Beljonne, J. Phys. Chem. A **113**, 2677 (2009).
- ⁴M. J. McIntire, E. S. Manas, and F. C. Spano, J. Chem. Phys. **107**, 8152 (1997).
- ⁵E. S. Manas and F. C. Spano, J. Chem. Phys. **109**, 8087 (1998).
- ⁶J. Cornil, D. A. dos Santos, X. Crispin, R. Silbey, and J. L. Brédas, J. Am. Chem. Soc. **120**, 1289 (1998).
- ⁷D. Beljonne, J. Cornil, R. Silbey, P. Millié, and J. L. Brédas, J. Chem. Phys. **112**, 4749 (2000).
- ⁸W. Barford, J. Chem. Phys. **126**, 134905 (2007).
- ⁹W. Barford and X. Xu, J. Chem. Phys. **128**, 034705 (2008).
- ¹⁰W. J. D. Beenken and T. Pullerits, J. Phys. Chem. B **108**, 6164 (2004).
- ¹¹J. Rissler, Chem. Phys. Lett. **395**, 92 (2004).
- ¹²A. V. Malyshev and V. A. Malyshev, Phys. Rev. B **63**, 195111 (2001).
- ¹³L. T. Liu, D. Yaron, M. I. Sluch, and M. A. Berg, J. Phys. Chem. B **110**, 18844 (2006).
- ¹⁴D. E. Logan and P. G. Wolynes, Phys. Rev. B **36**, 4135 (1987).
- ¹⁵A. Szabo and N. S. Ostlund, *Modern Quantum Chemistry*, (Dover Publications, Mineola, 1996).
- ¹⁶W. Barford and N. Paiboonvorachat, J. Chem. Phys. **129**, 164716 (2008).
- ¹⁷M. Chandross and S. Mazumdar, Phys. Rev. B **55**, 1497 (1997).
- ¹⁸S. Abe, J. Yu, and W. P. Su, Phys. Rev. B **45**, 8264 (1992); A. Abe, in *Relaxation in Polymers*, edited by T. Kobayashi (World Scientific, Singapore, 1993).
- ¹⁹W. Barford, R. J. Bursill, and R. W. Smith, Phys. Rev. B **66**, 115205 (2002).
- ²⁰W. Barford, *Electronic and Optical Properties of Conjugated Polymers* (Oxford University Press, Oxford, 2005).
- ²¹In the case of poly(para-phenylene) the appropriate local basis are the π -molecular orbitals of the benzene ring repeat unit (Ref. 16).
- ²²Analogous real-space representations of exciton wave functions have also been computed using atomic-orbital transition densities. [See J. Rissler, H. Bäessler, F. Gebhard, and P. Schwerdtfeger, Phys. Rev. B **64**, 045122 (2001); S. Tretiak and S. Mukamel, Chem. Rev. **102**, 3171 (2002); M. Sun, P. Kjellberg, W. J. D. Beenken, and T. Pullerits, Chem. Phys. **327**, 474 (2006).] The diagonal component of two-dimensional plots of the atomic transition densities represent the center-of-mass wave function, while the antidiagonal component represents the relative wave function.
- ²³M. J. Frisch, G. W. Trucks, H. B. Schlegel, G. E. Scuseria, M. A. Robb, J. R. Cheeseman, J. A. Montgomery, Jr., T. Vreven, K. N. Kudin, J. C. Burant, J. M. Millam, S. S. Iyengar, J. Tomasi, V. Barone, B. Mennucci, M. Cossi, G. Scalmani, N. Rega, G. A. Petersson, H. Nakatsuji, M. Hada, M. Ehara, K. Toyota, R. Fukuda, J. Hasegawa, M. Ishida, T. Nakajima, Y. Honda, O. Kitao, H. Nakai, M. Klene, X. Li, J. E. Knox, H. P. Hratchian, J. B. Cross, V. Bakken, C. Adamo, J. Jaramillo, R. Gomperts, R. E. Stratmann, O. Yazyev, A. J. Austin, R. Cammi, C. Pomelli, J. W. Ochterski, P. Y. Ayala, K. Morokuma, G. A. Voth, P. Salvador, J. J. Dannenberg, V. G. Zakrzewski, S. Dapprich, A. D. Daniels, M. C. Strain, O. Farkas, D. K. Malick, A. D. Rabuck, K. Raghavachari, J. B. Foresman, J. V. Ortiz, Q. Cui, A. G. Baboul, S. Clifford, J. Cioslowski, B. B. Stefanov, G. Liu, A. Liashenko, P. Piskorz, I. Komaromi, R. L. Martin, D. J. Fox, T. Keith, M. A. Al-Laham, C. Y. Peng, A. Nanayakkara, M. Challacombe, P. M. W. Gill, B. Johnson, W. Chen, M. W. Wong, C. Gonzalez, and J. A. Pople, GAUSSIAN 03.R.D02.
- ²⁴P. W. Atkins and R. S. Friedman, *Molecular Quantum Mechanics* (Oxford University Press, Oxford, 2004).
- ²⁵P. W. Atkins and J. de Paula, *Atkins' Physical Chemistry* (Oxford University Press, Oxford, 2006).
- ²⁶G. Rossi, R. R. Chance, and R. Silbey, J. Chem. Phys. **90**, 7594 (1989).
- ²⁷A. Tomlinson and D. Yaron, J. Comput. Chem. **24**, 1782 (2003).
- ²⁸Note that off-diagonal disorder in the π -electron system affects both the diagonal and off-diagonal disorder in the exciton model.
- ²⁹B. Kramer and A. MacKinnon, Rep. Prog. Phys. **56**, 1469 (1993).
- ³⁰M. P. Nightingale, V. S. Viswanath, and G. Müller, Phys. Rev. B **48**, 7696 (1993).
- ³¹The tridiagonal matrix was diagonalized by the *dsteV* routine supplied by LAPACK.
- ³²U. Rauscher, H. Bäessler, D. D. C. Bradley, and M. Hennecke, Phys. Rev. B **42**, 9830 (1990).